
Article
Open Access
MULTISCIA
JOURNALS PUBLISHERS
FRONTIERS IN
PHARMACEUTICAL ANALYSIS
ISSN: (3065- 1352)
https://multisciajournals.com/
journals/index.php/fpa
editor.fpa1@gmail.com

Frontiers in Zoological Research
Volume 1 Issue 1 2025

In Apostichopus japonicus, apoptosis controls intestinal regeneration through iPLA2 and EGFL7 signaling.

VV Subba Rao, W Golding
Department of **Zoological Research**

Article Info

Received: 30-12-2024 Revised:08-01-2025 Accepted:19-01-2025 Published:29-01-2025

ABSTRACT

By eliminating damaged or superfluous cells, apoptosis maintains organismal homeostasis. There is growing evidence that apoptosis also promotes tissue remodeling and activates regenerative pathways. However, the regulatory mechanisms that connect this type of planned cell death to regeneration are still not well understood, especially in animals that are evolutionarily basal. This study found strong apoptotic activity throughout important regenerative stages in the sea cucumber (Apostichopus japonicus), a model for intestinal regeneration. Intestinal regeneration was severely hampered by pharmacological suppression of apoptosis during wound healing and mesenteric scaffold development. Ca2+-independent phospholipase A2 (iPLA2), an enzyme that is normally up-regulated during successful regeneration, was significantly suppressed in the coordinated down-regulation of lipid metabolic pathways under apoptosis-inhibited conditions, according to quantitative proteomics using direct data-independent acquisition (DIA). Parallel to this, apoptotic blocking significantly decreased the expression of regeneration-associated proteins WNT6 and EGFL7. Reduced proliferative activity inside the regenerating intestinal primordia and poor mesenteric outgrowth were the outcomes of targeted inhibition of iPLA2, EGFL7, or WNT6. All of these results point to two possible mechanisms: apoptosis-dependent stimulation of WNT6/EGFL7 signaling and apoptosis-mediated restoration of lipid metabolism through iPLA2. This work broadens the conceptual framework of programmed cell death in tissue renewal and offers mechanistic insight into apoptosis-coupled regeneration mechanisms in basal deuterostomes.

Keywords: Direct; Intestinal regeneration; Apoptosis
Apostichopus japonicus, iPLA2, DIA proteomics, and EGLF7

OVERVIEW

From primitive invertebrates to amphibians and mammals, regeneration—the capacity to replace lost or injured tissues—is a conserved biological phenomenon (Maden, 2018). But along the evolutionary continuum, this ability gradually decreases, with lesser invertebrates typically having greater regenerative capability than more complex vertebrates (Hayat et al., 2022; Maden, 2018). More tissue specialization and architectural complexity in evolutionarily advanced species have been connected to this loss, according to recent data (Brockes & Kumar, 2008; Medina-Feliciano & García-Arrarás, 2021; Yuan et al., 2018). To yet, only evolutionarily primitive animals have shown robust and full regeneration in response to pathological harm. Some notable examples include intestinal regeneration in sea cucumbers (García-Arrarás et al., 2019; Zeng et al., 2023), head regeneration in Hydra species (Galliot & Chera, 2010), tail regeneration in Xenopus laevis tadpoles (Tseng et al., 2007), and whole-body regeneration in planarians from tissue fragments (Sánchez Alvarado, 2006). These models hold significant translational importance

for regenerative medicine and offer potent experimental tools for clarifying fundamental concepts of tissue regeneration. Through the targeted phagocytic clearance of damaged, defective, or redundant cells, apoptosis is a closely controlled type of programmed cell death that is necessary for preserving tissue homeostasis in multicellular animals (Elmore, 2007; Boada-Romero et al., 2020). There is increasing evidence that it plays important regulatory roles in beginning tissue remodeling and regeneration across a variety of taxa in addition to its traditional involvement in cellular turnover (Guerin et al., 2021; Vriz et al., 2014).
Accepted: July 02, 2025; Online: July 03, 2025; Received: May 26, 2025 Items for the foundation: The National Natural Science Foundation provided funding for this study.

Throughout regenerative processes, such as whole-body regeneration in planarians (Pellettieri et al., 2010), tail restoration in Xenopus laevis tadpoles (Tseng et al., 2007), head regeneration in Hydra species (Böttger & Alexandrova, 2007), and liver repair in mice (Li et al., 2010), elevated apoptotic activity has been consistently documented. Apoptotic pathway disruption hinders regeneration results. For example, Xenopus laevis tadpoles' tail regeneration is compromised when apoptosis is suppressed (Tseng et al., 2007), and Casp3−/− or Casp7−/− mice show delayed cutaneous wound healing and reduced liver regeneration (Li et al., 2010). Apoptosis mechanistically aids in regeneration by modifying important signaling pathways. While caspase3/7-mediated cell death in mammals encourages the release of arachidonic acid, which is then metabolized into PGE2 to promote stem cell proliferation and tissue repair (Li et al., 2010), apoptotic cells in Hydra species drive Wnt3 activation necessary for head regeneration (Chera et al., 2009). Through the selective release of bioactive compounds and vesicles, apoptotic cells also actively participate in intercellular communication. For instance, it has been demonstrated that apoptotic extracellular vesicles stimulate the release of growth factors like hepatocyte growth factor (HGF) and vascular endothelial growth factor (VEGF) (Brandel et al., 2022), and that lysophosphatidylinositol released by apoptotic cells improves migratory responses (Lauber et al., 2003). The molecular mechanisms underlying apoptosis-regulated regeneration are still poorly understood in evolutionarily primitive organisms with strong regenerative capacities, like echinoderms, where mechanistic studies are few and mostly restricted to descriptive phenotypic analyses. This is in spite of the advancements and insights gained from mammalian models. Phylogenetically close to chordates, echinoderms are an important group of invertebrates that share important evolutionary and developmental traits with vertebrates (García-Arrarás et al., 2019). Therefore, research on echinoderm regeneration—specifically, intestinal regeneration in sea cucumbers—can yield important theoretical insights related to regenerative medicine and human disease. The ability of sea cucumbers to regenerate their whole gastrointestinal architecture after evisceration is unique among echinoderms; most invertebrate phyla and higher vertebrates only show localized epithelium renewal in response to injury. This ability makes sea cucumbers an effective model for analyzing the molecular and cellular processes that underlie the regeneration of visceral organs (García-Arrarás et al., 2019). After being eviscerated, sea cucumbers' digestive systems fully recover their functionality in about a month. Mesenteric wound healing (0–2 days post-evisceration (dpe)), distal mesenteric expansion (7 dpe), luminal primordium

establishment (12 dpe), and lumen maturation (20 dpe) are the separate morphological steps that comprise the regeneration process. Rapid mesothelial repair at the ruptured mesentery starts the regeneration process. This creates a temporary regenerative primordium that synchronizes various cellular processes, such as migration, apoptosis, proliferation, differentiation, and dedifferentiation, to rebuild functional enteric tissues (Eisapour et al., 2021; Quispe-Parra et al., 2021; Zeng et al., 2023). It has been demonstrated that intestinal elongation and primordium development are driven by mesothelial cell migration and dedifferentiation (San Miguel-Ruiz & García-Arrarás, 2007). Mechanistic Wnt/β-catenin and FGF signaling have emerged as important regulatory axes in studies that have mostly concentrated on proliferative and dedifferentiation programs that enable tissue 2024). This study systematically investigated the functional relevance of apoptosis during digestive tract regeneration in A. japonicus in order to elucidate the cellular and molecular mechanisms underlying this process. Persistent apoptotic activity was found during important regenerative stages by comprehensive profiling. intestine reconstruction was significantly hampered by pharmacological prevention of apoptosis, suggesting that intestine regeneration requires programmed cell death. Possible apoptotic pathways involved in coordinating intestinal restoration were highlighted by comparative proteomic analysis using direct data-independent acquisition (DIA), which also showed significant differences in protein expression profiles and changes in signaling pathways between the apoptosis-inhibited and normally regenerating groups. These discoveries expand the conceptual framework for regenerative biology and offer crucial mechanistic insights into organ regeneration driven by apoptosis.

SUPPLIES AND TECHNIQUES

Experimental design and animals
We purchased adult A. japonicus individuals from Dalian Pacific Aquaculture (Dalian, Liaoning, compound, Sakura Finetek, 4583, USA).
To look into the role that apoptosis plays in reconstitution (Auger et al., 2023; Zeng et al., 2023). On the other hand, nothing is known about how apoptosis contributes to regenerative morphogenesis. While dedifferentiation and proliferation characteristics in Holothuria glaberrima have been linked to apoptosis (Reyes-Rivera et al., 2024), the molecular mechanisms underlying these effects are still mostly unknown. This information gap is especially noticeable in Apostichopus japonicus, where the mechanistic function of apoptosis in intestine regeneration is still unknown. This species is particularly well-suited for studying apoptotic signaling processes that control organ-level tissue regeneration because of its strong regenerative potential and quick timeline, even though it has been used as a comparative model for immunological investigations related to apoptosis (Tu et al.,

China) with a mean body weight of 110±5 g. Animals were acclimated for seven days before the experiment in a recirculating artificial seawater system that was kept at 11°C, salinity 28–30°, pH 8.1–8.3, and constant aeration (dissolved oxygen >6 mg/L). A 3 mL intracoelomic injection of 0.35 mol/L KCL (Sigma-Aldrich, P9541, USA) per 100 g body weight was used to produce evisceration (Quispe-Parra et al., 2021; Zeng et al., 2023). To guarantee uniformity throughout individuals, the complete ejection of internal organs (such as the intestines and respiratory tree) was physically verified. The Institutional Animal Care and Use Committee gave its approval to all procedures (Protocol #IACUC-2023-019). 135 animals were randomly assigned to five experimental cohorts (n=27 per group) in order to assess the spatiotemporal dynamics of apoptosis. Four regeneration groups were sampled at 2, 7, 12, and 20 dpe, and one intact control group (non-eviscerated; normal) was also included. Nine animals were sacrificed for each group at each time point. Tissues were used for western blotting (n=3; protein extracted using RIPA lysis buffer), flow cytometry (n=3; cell suspensions made by collagenase IV digestion), and frozen sectioning (n=3; embedded in OCT

regeneration, 288 animals were randomly assigned to two treatment groups (*n*=3 biological replicates per group, 48 individuals per replicate): a control group receiving 0.1% dimethylsulfoxide (DMSO, final concentration in coelomic fluid) and a Z-VAD-FMK (Z-VAD) treatment group administered Z- VAD (final concentration 100 μmol/L; MCE, HY-16658, USA; dissolved in DMSO). Initial treatment was administered at 6 h post-evisceration (hpe) via intracoelomic injection using 25G needles (BD Biosciences, 305122, USA) at a volume of 100 μL, with booster injections administered at 24 h intervals to maintain effective drug levels until sampling. Regenerating intestinal tissues were collected at 2, 7, and 12 dpe. At each time point, tissues from three animals were used for flow cytometry to assess inhibition efficiency; tissues from another three animals were used for frozen sectioning; tissues from six animals were used for RNA and protein extraction; and tissues from an additional six animals (100 mg each) were snap- frozen in liquid nitrogen and stored at −80°C for proteomic analysis.

To validate the phenotypic effects of Z-VAD-mediated apoptosis inhibition, 54 specimens were randomly allocated into negative control (NC) and siCaspase3 treatment groups (*n*=3 biological replicates per group, 18 individuals per replicate). At 2, 7, and 12 dpe, nine animals per group were sacrificed for frozen sectioning, and six animals per group were used for RNA and protein extraction.

To evaluate the role of candidate genes identified through proteomic screening (iPLA2, WNT6, and EGFL7) in intestinal regeneration, animals were allocated as follows. For independent phospholipase A2 (iPLA2) validation, 54 specimens were randomly assigned to NC and FKGK18 treatment groups (*n*=3 biological replicates per group, 18 individuals per replicate). Intestinal primordia were collected at 2, 7, and 12 dpe. Nine animals per group were used for frozen sectioning, and six animals for RNA and protein extraction. For EGFL7 validation, 54 animals were randomly assigned to NC and siEGFL7 groups (*n*=3 biological replicates per group, 18 individuals per replicate). Six animals per group were processed for RNA and protein extraction for western blotting and quantitative real-time PCR (qPCR), while regenerated tissues from nine animals per group were collected at 2, 7, and 12 dpe for frozen sectioning. For WNT6 validation, 54 animals were randomly allocated into NC and siWNT6 groups (*n*=3 biological replicates per group, 18 individuals per replicate). At 2, 7, and 12 dpe, tissues from nine animals per group were collected for frozen sectioning, and six animals per group were used for RNA and protein extraction for western blotting and qPCR.

Apoptosis detection

Apoptotic cells were identified using a One Step TUNEL Apoptosis Assay Kit (Beyotime, China), which labels DNA strand breaks at exposed 3'-OH termini with fluorescein isothiocyanate-labeled dUTP (FITC-dUTP) catalyzed by terminal deoxynucleotidyl transferase (TdT). Apoptotic cells exhibiting green fluorescence were visualized by fluorescence microscopy or flow cytometry.

For immunofluorescence analysis, animals were dissected along the dorsal midline to expose the digestive tract. The anterior mesentery and associated regenerative primordia were excised with surgical clippers and embedded in Tissue- Tek O.C.T. Compound (Sakura, Cat#4583, USA). Samples were snap-frozen in liquid nitrogen, and 6 μm sections were prepared using a freezing microtome (DAKEWE, China). Sections were fixed in 4% paraformaldehyde for 30 min, washed in phosphate-buffered saline (PBS), and permeabilized with 0.3% Triton X-100 in PBS for 10–15 min. After additional PBS washes, sections were incubated with freshly prepared TUNEL reagent (45 μL of FITC-dUTP mixed with 5 μL of TdT) for 60 min at 37°C in the dark. Following washing with PBS, nuclei were stained with 4′,6-diamidino-2- phenylindole (DAPI) for 10 min. Sections were examined and photographed under a fluorescence microscope (Zeiss,

Germany). To quantify the apoptotic rate in regenerating primordia, TUNEL and DAPI fluorescence intensities were measured in at least three non-adjacent sections using ImageJ. The relative apoptotic ratio (%) was expressed as the ratio of TUNEL fluorescence intensity to DAPI fluorescence intensity. The area of regenerative primordia was determined based on DAPI staining using ImageJ.

For flow cytometric quantification, regenerating tissues were finely minced and enzymatically dissociated using type IV collagenase and trypsin until a single-cell suspension was obtained through filtration with a 300-mesh sieve. Digestion was terminated with serum, and cells were pelleted by centrifugation at 800 ×*g*, 16°C for 5 min. Pellets were fixed in 4% paraformaldehyde for 15 min at room temperature, followed by PBS washing and permeabilization with 0.3% Triton X-100 in PBS for 10 min. Cells were then incubated with freshly prepared TUNEL solution (90 μL of FITC-dUTP with 10 μL of TdT) for 1 h on a vertical shaker protected from light. After washing with PBS, cells were resuspended in 400 μL of PBS for analysis. All staining steps were performed in darkness to preserve fluorescence.

Western blotting

Total proteins were extracted from regenerating intestinal tissue using a commercial total protein extraction kit (Sangon, China), and protein concentrations were determined using a bicinchoninic acid (BCA) assay kit (Sangon, China). Equal amounts of protein (50 μg per sample) were separated by sodium dodecyl sulfate-polyacrylamide gel electrophoresis (SDS-PAGE) and transferred onto polyvinylidene difluoride (PVDF) membranes. For low molecular weight proteins, 15% SDS-PAGE gels and 0.22 μm PVDF membranes were used. Membranes were blocked with 5% non-fat milk in Tris-buffered saline with 0.5% Tween-20 (TBST; 50 mmol/L Tris-HCl, 150 mmol/L NaCl, 0.5% Tween-20) at 25°C for 2 h. Primary antibodies were applied overnight at 4°C, including anti- Ajcaspase-3 rabbit antibody (1:1 000, Sangon, D220074, China), anti-Ajcaspase8 rabbit antibody (1:1 000, ABclonal, A0215, China), anti-AjBax rabbit antibody (1:1 000, GenScript Technology, USA), anti-AjEGFL7 rabbit antibody (1:500, ABclonal, A9376, China), anti-AjWNT6 mouse antibody (1:400, 1P89831, Baijia, China), anti-AjiPLA2 rabbit antibody (1:500, 22030-1-AP, Proteintech, USA), and anti-Ajβ-tubulin mouse antibody (1:5 000, ABclonal, AC021, China). After washing, membranes were incubated with horseradish peroxidase (HRP)-conjugated secondary antibodies: goat anti- rabbit IgG (1:5 000, Sangon, D110058, China) or goat anti- mouse IgG (1:5 000, Sangon, D110087, China) for 2 h at 25°C. Membranes were washed three times (10 min each) with TBST, incubated with enhanced chemiluminescence (ECL) reagent, and imaged using a chemiluminescence system (Bio-Rad, USA). Band intensities were quantified using ImageJ software. All results represent three independent

experimental replicates.

Pharmacological and genetic interference

Z-VAD (MCE, HY-16658, USA), an irreversible pan-caspase inhibitor targeting caspase-1, -3, -7, -8, -9, and -10, was used to suppress apoptosis in *A. japonicus*. In brief, Z-VAD was dissolved in DMSO to prepare a 100 mmol/L stock solution. Cytotoxicity was evaluated at concentrations of 0, 10, 20, 50, 100, and 200 μmol/L using an MTT Cell Proliferation and Cytotoxicity Assay Kit (Beyotime, C0009, China). Caspase-3 activity was quantified using a Caspase-3 Activity Assay Kit (Beyotime, C1115, China). Based on viability and inhibition efficiency, 100 μmol/L Z-VAD was selected as the optimal working concentration. Z-VAD was administered intracoelomically at a final concentration of 100 μmol/L, with the first treatment delivered 6 hpe, followed by daily luminal injections at 24 h intervals. Inhibition of apoptosis was verified by TUNEL staining in tissue sections and flow cytometry.

FKGK18, a fluoroketone-based selective inhibitor of Ca^{2+}- iPLA2, was dissolved in DMSO to generate a 10 mmol/L stock solution. Cytotoxicity was evaluated at concentrations of 0, 5, 10, 20, and 50 μmol/L using an MTT Cell Proliferation and Cytotoxicity Assay Kit (Beyotime, C0009, China). Inhibition efficiency was confirmed by quantifying iPLA2 mRNA and protein expression via western blotting and qPCR. FKGK18 was administered intracoelomically at a working concentration of 10 nmol/L, providing the optimal inhibitory effect without impacting cell viability. Injection timing and grouping criteria were consistent with those used in the Z-VAD experiments.

Sequence-specific small interfering RNAs (siRNAs) targeting epidermal growth factor-like domain 7 (*EGFL7*), *WNT6*, and *caspase-3* (si*EGFL7*, si*WNT6*, and si*Caspase3*, respectively) were synthesized by GenePharma along with a non-targeting negative control siRNA (siNC; sequences provided in Table 1). For *in vivo* administration, transfection complexes were prepared by mixing 80 μL of PBS with 10 μL of each siRNA (20 μmol/L; si*EGFL7*, si*WNT6*, si*Caspase3,* or siNC) and 10 μL of Lipo6000™ Transfection Reagent (Beyotime, China). Each experimental group comprised three biological replicates (*n*=3 individuals per replicate). During intestinal regeneration, experimental solutions were administered to individual sea cucumbers by intramuscular injection at 48 h intervals, beginning at 6 hpe and continuing until 10 dpe. Tissue samples were collected at defined regenerative stages (2, 7, and 12 dpe) to monitor morphogenetic progression.

Protein preparation and quality control

Fresh tissue specimens (100 mg per group) were immediately flash-frozen in liquid nitrogen and pulverized using a cryogenic grinding system (SPEX SamplePrep 6970 EFM). Approximately 100 mg of powdered tissue was transferred into
2 mL polycarbonate centrifuge tubes (Beckman Coulter, 357448, USA) prechilled with liquid nitrogen. Protein lysis was performed by adding 1 mL of SDT buffer (4% SDS, 100 mmol/L NaCl, 100 mmol/L Tris-HCl pH 8.0) supplemented with(Sorvall ST 40R, Germany, F15-8x50cy rotor). The clarified supernatant was alkylated with 50 mmol/L iodoacetamide (Sigma-Aldrich, I1149, USA) in the dark for 1 h at 25°C. Protein precipitation was achieved by adding four volumes of prechilled (−20°C) acetone (Merck, 100014, Germany), followed by incubation at −20°C for 2 h. Precipitated proteins were pelleted by centrifugation (12 000 ×*g*, 15 min, 4°C), washed twice with 1 mL of ice-cold acetone, and air-dried for 15 min in a chemical fume hood.

Dried protein pellets were dissolved in dissolution buffer (8 mol/L urea, 2 mol/L thiourea, 4% CHAPS, 50 mmol/L triethylammonium bicarbonate (TEAB), pH 8.5) and incubated at 37°C for 2 h with gentle agitation. Protein concentration was quantified using a Qubit 4.0 Fluorometer (Thermo Fisher, Q33238, USA) with the Qubit Protein Assay Kit according to the manufacturer's instructions. Protein integrity was verified by

SDS-PAGE and Coomassie Brilliant Blue R-250 staining. Trypsin digestion was performed as described previously (Zeng et al., 2025) using sequencing-grade modified trypsin (Promega, V5280, USA) at an enzyme-to-protein ratio of 1:50 (w/w).

Liquid chromatography-tandem mass spectrometry (LC- MS/MS) in DIA mode

Peptide samples were analyzed using a Vanquish Neo ultra- high-performance liquid chromatography (UHPLC) system (Jones et al., 2014) coupled to a Thermo Orbitrap Astral mass spectrometer (USA). Separation was performed using a C18 pre-column (17450; 0.5 mm×300 μm, 5 μm, Thermo, USA) maintained at 50°C and an analytical C18 column (ES906; PepMap Neo UHPLC 150 μm×15 cm, 2 μm, Thermo, USA). Mass spectrometry was carried out with an Easy-Spray (ESI) ion source (spray voltage 1.9 kV; ion transfer tube temperature 290°C). Mass spectra were acquired in DIA mode. The primary scan range was m/z 380–980, with a resolution of 240 000 (at m/z 200). DIA settings included a parent ion window size of freshly prepared 10 mmol/L DTT (Biosharp, BL102A, China), followed by vigorous vortexing (2 000 r/min, 30 s) and ultrasonic disruption (Branson Sonifier 450, USA, amplitude, five cycles of 30 s pulse/30 s rest) in an ice-water bath.

The homogenate was heat-denatured at 95°C for 10 min (ThermoMixer C, Eppendorf, Germany), rapidly cooled on ice for 2 min, and centrifuged at 12 000 ×*g* for 15 min at 4°CProtein quantification was statistically assessed using Student's *t*-test. Proteins exhibiting significant differences between experimental and control groups (P<0.05, $|\log_2 FC|$>1 [fold change (FC)>2.0 or<0.5]) were defined as differentially expressed proteins (DEPs).

2 Th, 300 DIA windows, normalized collision energy (NCE) of 25%, secondary m/z acquisition range of 150–2 000, sub-ion resolution of 80 000, and maximum injection time of 3 ms.

Protein identification and quantification

Raw mass spectrometry data were processed using the DIA- NN library search software. Search parameters included a precursor ion mass tolerance of 10 ppm and fragment ion mass tolerance of 0.02 Da. To enhance data reliability, peptide spectrum matches (PSMs) with confidence scores ≥ 99% were retained, and only peptides and proteins meeting these criteria were used for downstream analysis. Identifications with a false discovery rate (FDR) >1% (Global.*Q*-value<0.01; PG.*Q*-value<0.01) were excluded. Total intensity normalization was applied to correct for variations in sample loading and instrument response. Briefly, for each sample, the total peptide peak area was calculated and normalized to the maximum total intensity across all samples using the formula:

$$10\%\text{ormalizationratio} = \text{MaximumTotalIntensity}/\text{SampleTotalIntensity} \quad (1)$$

Functional annotation and differential expression analysis Comprehensive functional annotation of proteins and DEPs was performed using an integrated bioinformatics pipeline. Gene Ontology (GO) annotations were assigned via InterProScan (v.5.52-86.0) using default settings, integrating six major protein signature databases: Pfam (v.35.0) for domain identification, PRINTS (v.42.0) for motif recognition, ProDom (v.2012.1) for family classification, SMART (v.7.1) for domain architecture analysis, PROSITE (v.20.132) for functional site detection, and PANTHER (v.16.0) for evolutionary classification (Huang et al., 2009).

DEPs were identified using DESeq2 (v.1.30.1), applying a significance threshold of $|\log_2(\text{fold change})|>1$ and adjusted $P<0.05$. Hierarchical clustering of DEPs was performed using the pheatmap package (v.1.0.12) in R, employing Euclidean distance and complete linkage to visualize expression profiles across experimental conditions.

Functional enrichment analysis included both GO term (Biological Process (BP), Molecular Function (MF), Cellular Component (CC)) and Kyoto Encyclopedia of Genes and Genomes (KEGG) pathway (release 97.1) enrichment analyses, conducted using clusterProfiler (v.4.0.5). Statistical significance was determined using a hypergeometric test with Benjamini-Hochberg correction (FDR<0.05). All visualizations were generated using ggplot2 (v.3.3.5) with custom color palettes for scientific presentation (Jones et al., 2014).

qPCR

Total RNA was extracted from tissues collected in parallel with those used for proteomic sequencing. Extracted RNA was reverse transcribed into cDNA, which served as the template for qPCR. RNA extraction, reverse transcription, and qPCR procedures followed previously published protocols (Guo et al., 2023, 2024). β-tubulin was used as the internal reference gene. Each experiment was independently replicated three times, with results reported as mean±standard deviation (SD) (Livak & Schmittgen, 2001). Relative transcript levels were calculated using the $2^{-\Delta\Delta CT}$ method. Statistical differences among treatment groups were denoted as *: $P<0.05$; **: $P<0.01$; ***: $P<0.001$.

Statistical analysis

All quantitative data are presented as mean±SD from three independent biological replicates. Pairwise comparisons were performed using unpaired two-tailed Student's *t*-test. For comparisons involving three or more groups, one-way analysis of variance (ANOVA) with Dunnett's *post hoc* test was used. A threshold of $P<0.05$ was considered statistically significant. All statistical analyses and graphical outputs were generated using GraphPad Prism v.7.0 (GraphPad Software, USA).

RESULTS

Apoptosis is significantly increased during intestinal remodeling

To investigate apoptotic involvement in intestinal regeneration, TUNEL *in situ* hybridization assays combined with DAPI nuclear counterstaining were performed on frozen mesenteric sections of *A. japonicus* collected at baseline and at 2, 7, 12, and 20 dpe. TUNEL-positive nuclei displayed green fluorescence under 450–500 nm excitation, while DAPI- stained nuclei displayed blue fluorescence under UV illumination. The relative apoptotic ratio (%) was quantified as the percentage of TUNEL to DAPI fluorescence intensity usingImageJ, with data expressed as mean±SD (Figure 1C). In intact mesentery, minimal apoptosis was observed (2.253%±1.974%) (Figure 1A, C). At 2 dpe, apoptotic cells were significantly elevated and predominantly localized to the mesentery and outer mesothelial layer of the regenerating rudiment, coinciding with early wound healing (Figure 1A). By
7 dpe, apoptosis further intensified (20.90%±3.35%) (Figure 1C) and remained confined to the mesothelial layer, corresponding to rudiment expansion and mesentery thickening

(Figure 1A). A peak apoptotic ratio was observed at 12 dpe (31.70%±3.02%) (Figure 1C), localized predominantly to the developing luminal epithelium during intestinal lumen formation (Figure 1A). Apoptotic activity subsequently declined by 20 dpe, returning to near-basal levels as the primary intestinal embryonic structure matured (Figure 1A, C). As intestinal regeneration progressed (Figure 1B), the number of TUNEL-positive cells increased sharply, reaching a peak at 12 dpe, followed by a decline to baseline levels by 20 dpe.

Western blot analysis of apoptosis-related proteins further supported these observations. Expression levels of key apoptotic regulators (Ajcaspase-3, Ajcaspase-8, and AjBax) were up-regulated during active regeneration, followed by a marked decline once the primary intestinal structure formed at 20 dpe (Figure 1E). Ajcaspase-8 and AjBax peaked at 7 dpe, whereas Ajcaspase-3 activity increased until reaching maximum expression at 12 dpe (Figure 1E), possibly indicating that distinct protein networks may regulate apoptosis at different morphogenetic stages. The dynamic expression of these proteins paralleled regeneration advancement, with peaks during critical morphogenetic periods and subsequent return to baseline, consistent with the spatiotemporal pattern observed in the TUNEL assay.

To assess apoptosis at the tissue level, regenerating samples were enzymatically dissociated using type IV collagenase and trypsin, followed by filtration through a 300- mesh sieve to obtain single-cell suspensions for TUNEL- based flow cytometry. This analysis confirmed the immunohistochemical data, revealing a distinct temporal pattern of apoptotic activity (Figure 1D). Compared with baseline levels in normal tissue (2.94%±0.41%), apoptosis increased markedly during early regeneration (2 dpe: 12.28%±3.59%), peaked at 7 dpe (17.18%±0.45%) and 12 dpe (28.23%±1.98%), and then declined to near-baseline levels by 20 dpe (6.0%±0.9%) (Figure 1D). Collectively, results from TUNEL staining, immunofluorescence, western blotting, and flow cytometry indicate that intestinal regeneration in *A. japonicus* is governed by tightly regulated apoptotic dynamics. The spatiotemporal activation of *Bax* and caspases, along with peak apoptotic activity during key morphogenetic stages (7–12 dpe), highlights a fundamental role for programmed cell death in coordinating tissue remodeling and organogenesis.

Apoptosis is required for regenerative rudiment remodeling

To determine whether apoptosis is functionally required for intestinal regeneration, the pan-caspase inhibitor Z-VAD was administered intracoelomically at 24 h intervals following evisceration. Apoptotic activity was assessed using flow cytometry and TUNEL-based fluorescence quantification using ImageJ, alongside morphometric measurements of regenerative primordia in frozen sections. Sustained Z-VAD treatment effectively suppressed apoptosis, reducing the

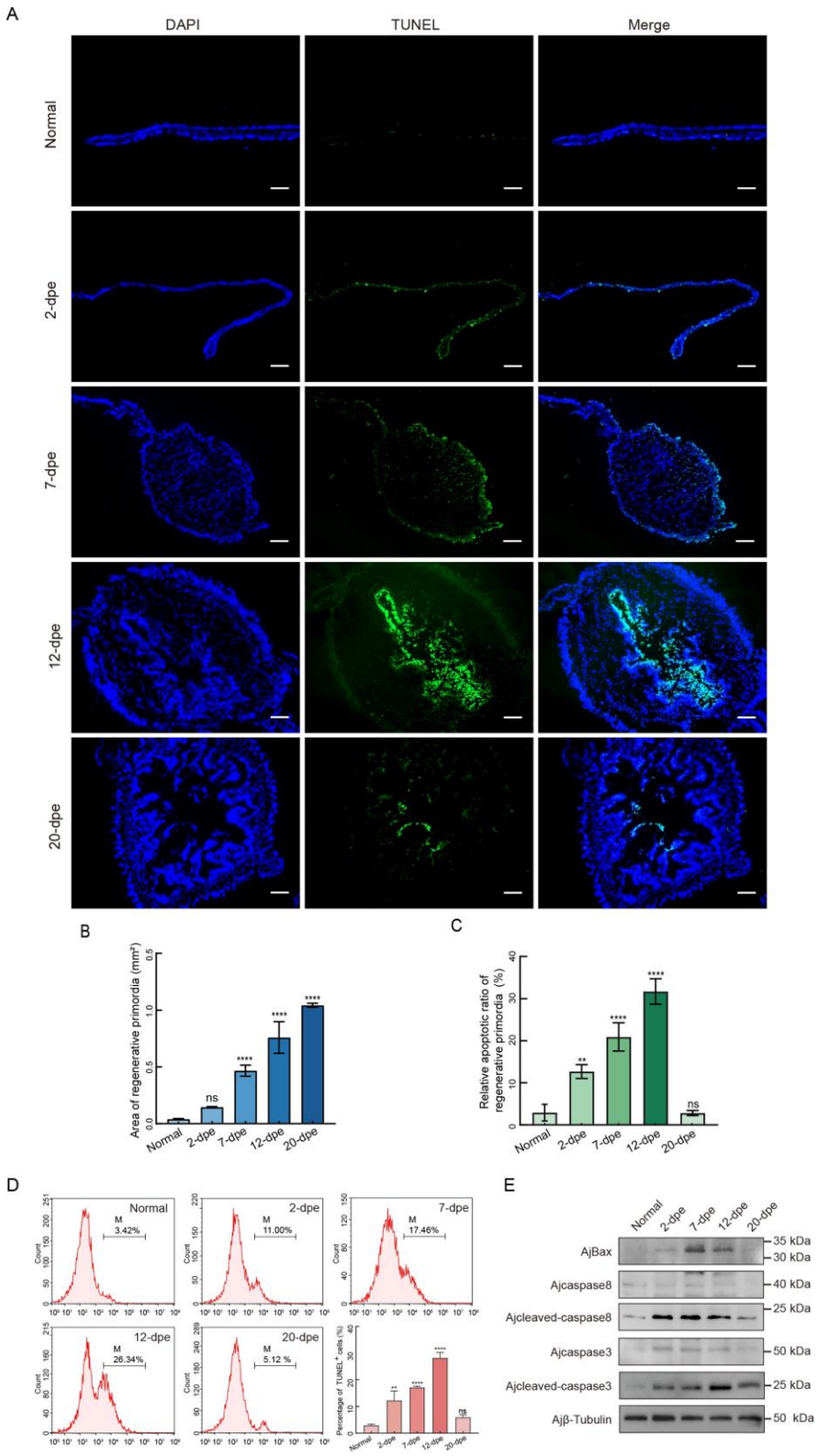

Figure 1 Up-regulation of cell apoptosis levels during intestinal regeneration

A: TUNEL assay was used to detect apoptosis levels in normal and regenerative stages (2–20 dpe). Dorsal mesentery sampling sites were stained for each regeneration stage. Blue denotes DAPI-stained nuclei; green denotes TUNEL-positive apoptotic cells. Scale bar, 200 μm. dpe: days post- evisceration. B: Quantification of regenerative primordia area

indicated by DAPI staining in A using ImageJ. C: Relative apoptotic ratio of regenerative primordia (%) in the normal and four regeneration groups, presented as a histogram. D: Apoptosis levels at regeneration time points were analyzed by flow cytometry. For each sample, 10 000 cellular events were collected; data represent three independent experiments and are shown as histograms. Statistical analyses represent mean±SD; ns: Not significant; *: P<0.05; **: P<0.01; ****: P<0.0001. E: Protein expression levels of AjBax, Ajcaspase-8, Ajcleaved-caspase-8, Ajcaspase-3, Ajcleaved-caspase-3, and Ajβ-tubulin (internal reference) in normal and regenerating tissues at four time points.

apoptotic index from 10.94%±0.31% to 3.47%±0.78% at 2 dpe. This inhibitory effect persisted at 7 dpe, with treated specimens exhibiting significantly lower apoptotic levels (5.39%±1.5%) compared with controls (18.70%±0.7%) (Figure 2A, B). In parallel, Z-VAD treatment led to significant down-regulation of *caspase-3* and *Bax* mRNA expression at 2, 7, and 12 dpe (Figure 2C, D). Histological analyses corroborated these findings, showing marked depletion of apoptotic cells in Z-VAD-treated tissues at 2, 7, and 12 dpe (Supplementary Figure S1B). Although Z-VAD had minimal effect on primordium area during early healing (2 dpe), it significantly impaired mesenteric expansion and delayed regeneration, with a 65% reduction in rudiment growth at 7 dpe (P<0.0001) and delayed lumen maturation at 12 dpe (Figure 2E; Supplementary Figure S1A). Similarly, siRNA-mediated knockdown of caspase-3 resulted in significant impairment of intestinal regeneration efficiency, including reduced regenerative primordia area and delayed lumen maturation, phenocopying the effects of Z-VAD (Supplementary Figure S2). Prolonged apoptotic inhibition disrupted normal tissue remodeling and prevented establishment of functional intestinal architecture, ultimately leading to incomplete organogenesis and death due to regeneration failure.

Direct DIA reveals apoptosis-related molecular alterations under Z-VAD treatment

To elucidate molecular alterations associated with Z-VAD- mediated apoptotic suppression, DIA proteomic analysis was conducted at 2 and 7 dpe across four experimental groups:
(1) 2 dpe control, (2) 2 dpe Z-VAD, (3) 7 dpe control, and (4) 7 dpe Z-VAD. Vehicle-injected controls were processed in parallel. The complete MS dataset is available in the iProX repository (Project ID: PXD057001).

Heatmap clustering and transcriptional validation confirmed effective suppression of apoptosis-related proteins following Z- VAD treatment. Key caspase family members, including *caspase-2*, *caspase-8*, and *caspase-6*, were significantly down-regulated in both 2 dpe and 7 dpe Z-VAD-treated groups compared with controls, while *Bcl-2* was up-regulated (Figure 3A). These patterns were corroborated by qPCR, which showed consistent reductions in *caspase-2*, *caspase-8*, and *caspase-6* mRNA, along with elevated *Bcl-2* expression (Figure 3B–E). Z-VAD treatment induced broad proteomic reprogramming. At 2 dpe, 155 proteins were down-regulated and 237 proteins were up-regulated compared to the controls. Strongly suppressed proteins included fatty acid-binding protein, brain (FABP7), zinc finger CCHC domain-containing protein 24 (ZCCHC24), bone morphogenetic protein 3 (BMP3), sulfotransferase 1 family member D1 (ST1D1), and ankyrin repeat domain-containing protein 54 (ANR54), whereas the most highly up-regulated proteins included carboxy-terminal kinesin 2 (CTK2), aquaporin-9 (AQP9), cornifelin homolog B (CNFNB), receptor-type tyrosine-protein phosphatase F-like isoform X1, and cell growth regulator with RING finger domain protein 1 (CGRF1). By 7 dpe, dysregulation intensified, with 214 proteins down-regulated and 200 up-regulated. Suppressed proteins included cubilin (CUBN), interferon-induced very large GTPase 1 (GVIN1), sushi, von Willebrand factor type A EGF and pentraxin domain-containing protein 1 (SVEP1), APOBEC1 complementation factor (A1CF), and fatty acid-binding protein (FABP6). Upregulated proteins included CTK2, L-

gulonolactone oxidase (GGLO), cytochrome P450 1A1 (CP1A1), neuron navigator 3 (NAV3), and putative amiloride- sensitive sodium channel subunit beta (Supplementary Table S1).

KEGG enrichment analysis of DEPs

To elucidate the biological pathways modulated by apoptosis during intestinal regeneration, KEGG enrichment analysis was performed on DEPs between Z-VAD-treated and control groups at corresponding time points. At 2 dpe, proteins up- regulated in the 2d_Z-VAD group were predominantly enriched in metabolic pathways, including phosphonate and phosphinate metabolism, ether lipid metabolism, and the pentose phosphate pathway. In contrast, down-regulated proteins were associated with essential signaling and metabolic pathways, notably the transforming growth factor β (TGF-β) signaling pathway, glutathione metabolism, and arachidonic acid metabolism (Figure 4A, B). At 7 dpe, the proteomic landscape exhibited more pronounced changes. Proteins up-regulated in the 7d_Z-VAD group were enriched in ascorbate and aldarate metabolism, thiamine metabolism, and ubiquitin-mediated proteolysis. Conversely, down-regulated proteins were primarily enriched in extracellular matrix (ECM) remodeling (ECM-receptor interaction), energy metabolism (glycolysis/gluconeogenesis), and metabolic regulation (retinol metabolism; glutathione metabolism) (Figure 4C, D).

GO analysis delineates functional specialization of apoptosis-modulated proteins

To further clarify the functional implications of apoptosis regulation during intestinal regeneration, GO enrichment analysis was conducted on DEPs across MF, BP, and CC categories. At 2 dpe, up-regulated proteins in Z-VAD-treated samples were enriched in terms related to single-organism cellular processes, membrane-related terms, and phospholipase A2 activity (Figure 5A), while down-regulated DEPs were associated with oxidation-reduction processes, extracellular region, and calcium ion binding (Figure 5B). At 7 dpe, up-regulated DEPs were enriched in single-organism processes, membrane-related functions, and receptor activity (Figure 5C), whereas down-regulated DEPs were enriched in tRNA metabolic processes, extracellular regions, and nucleic acid binding (Figure 5D).

Apoptosis inhibition suppresses regeneration-related protein expression

To explore the molecular mechanisms underlying the regulatory effect of apoptosis on intestinal regeneration, expression profiling of regeneration-associated proteins was conducted following apoptosis inhibition. Heatmap analysis revealed that Z-VAD-mediated apoptosis inhibition significantly down-regulated key developmental regulators, including protein WNT-6 (WNT6), EGFL7, growth factor receptor-bound protein 2 (GRB2), fibroblast growth factor receptor (FGFR), Ca^{2+}-iPLA2, and BMP3 (Figure 6A). QPCR analysis corroborated these findings, showing consistent down-regulation at the mRNA level for selected targets (*BMP3*: 2 dpe, $P<0.05$; 7 dpe, $P<0.05$; *WNT6*: 2 dpe, $P>0.05$; 7 dpe, $P<0.01$) (Figure 6B, C). Western blotting further confirmed that Z-VAD treatment significantly decreased iPLA2 and EGFL7 protein expression at 2 dpe and 7 dpe (Figure 6F). Temporal analysis of *EGFL7* and *iPLA2* expression during normal intestinal regeneration showed marked increases, peaking at 12 dpe, suggesting a functional role in *A. japonicus*

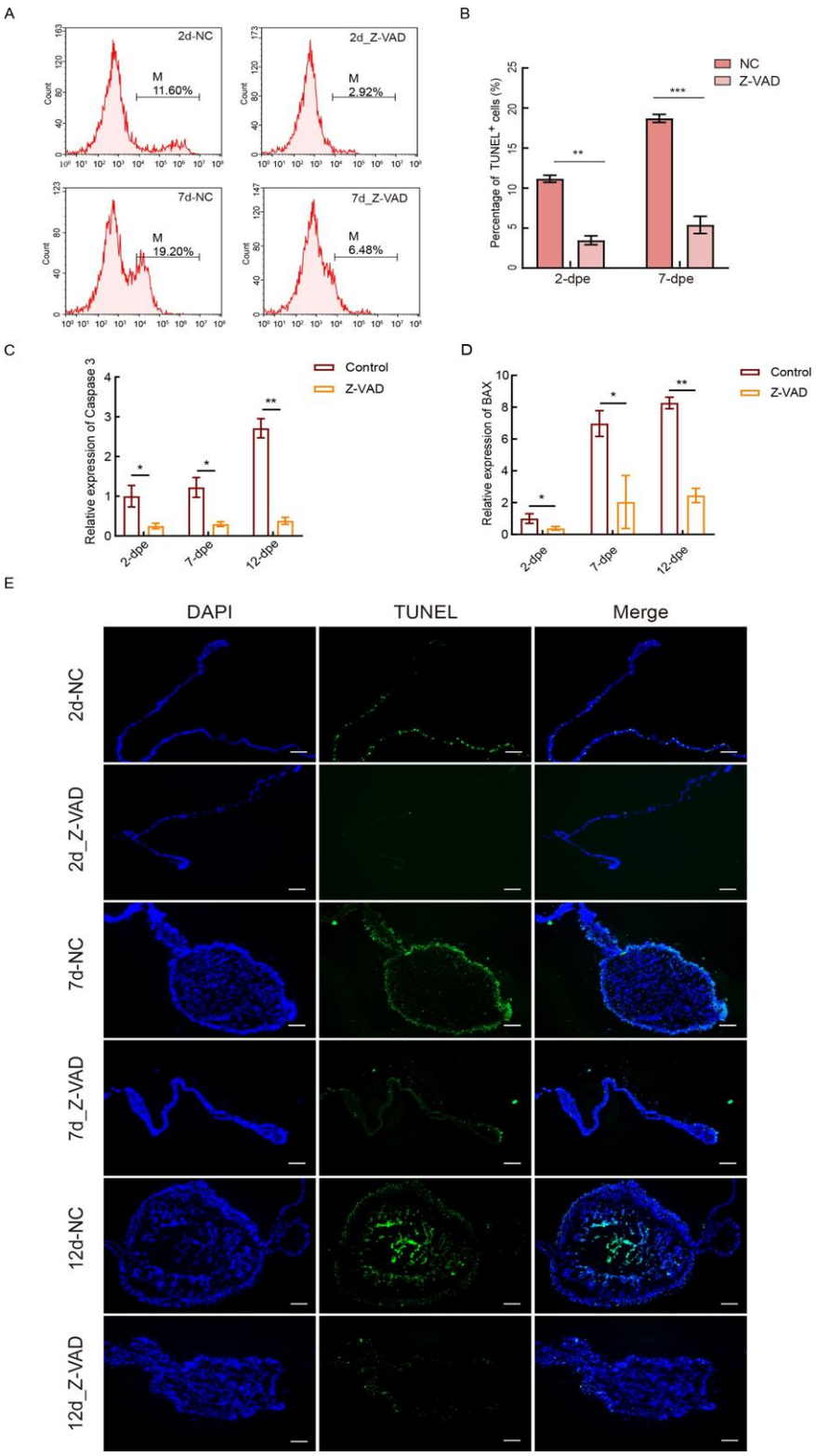

Figure 2 Inhibition of apoptosis delays intestinal regeneration

A: Apoptosis levels after Z-VAD treatment detected by flow cytometry; 10 000 cellular events per sample. B: Quantitative analysis of TUNEL- positive cells following Z-VAD treatment. C: qPCR analysis of *caspase-3* mRNA expression. D: qPCR analysis of *Bax* mRNA expression. E: Detection of intestinal regeneration and apoptosis after Z-VAD inhibition by TUNEL *in situ* hybridization; blue, DAPI-stained nuclei; green, TUNEL-positive cells. Scale bar: 200 μm. Statistical analyses represent mean±SD (n≥3 independent experiments); ns: Not significant; *: P<0.05; **: P<0.01; ***: P<0.001.

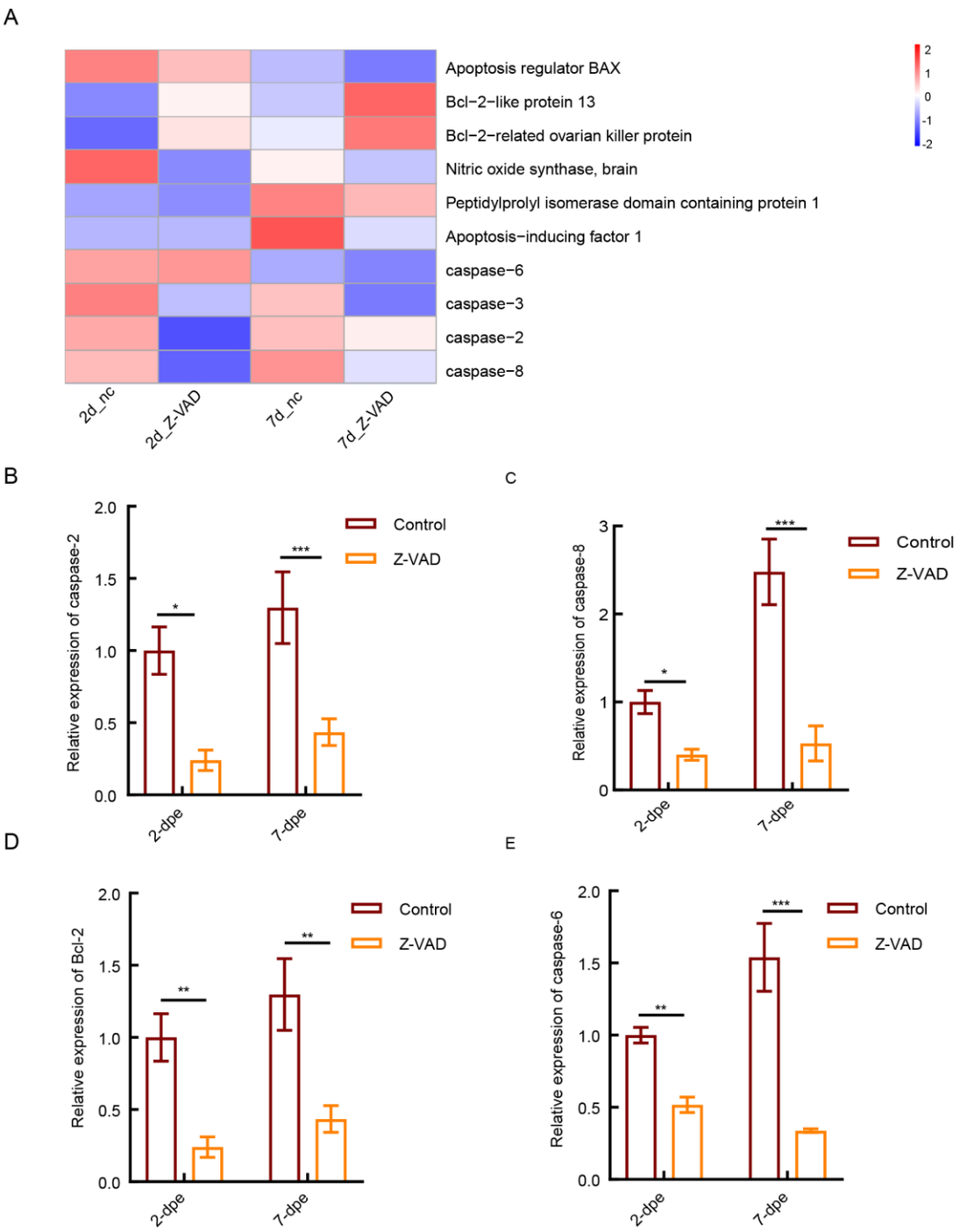

Figure 3 Expression pattern analysis of apoptosis-related proteins between Z-VAD-treated and control groups

A: Heatmap correlation analysis of apoptosis-related proteins. 2d_nc and 2d_Z-VAD denote 2d_control and 2d_Z-VAD groups, respectively; 7d_nc and 7d_Z-VAD denote 7d_control and 7d_Z-VAD groups, respectively. Z-VAD, apoptosis inhibitor. B: qPCR analysis of *caspase-2* mRNA. C: qPCR analysis of *caspase-8* mRNA. D: qPCR analysis of *Bcl-2* mRNA. E: qPCR analysis of *caspase-6* mRNA. Data represent mean±SD, n=3 independent individuals; ns: Not significant; *: P<0.05; **: P<0.01; ***: P<0.001

intestinal regeneration (Figure 6D, E). These results indicate that inhibition of apoptosis strongly affects the expression of regeneration-associated factors (such as EGFL7), key fatty acid metabolism protein iPLA2, and components of the WNT6 signaling pathway.

Targeted disruption of *iPLA2*, *EGFL7*, and *WNT6* impairs intestinal regenerative primordial remodeling

To functionally validate the pathways identified in proteomic screening, the roles of iPLA2, EGFL7, and WNT6 in intestinalregeneration were examined using pharmacological and genetic interventions. Apoptosis inhibition suppressed key components of fatty acid metabolism, including FABP7 and FABP6 at 2 dpe and 7 dpe, and significantly reduced KEGG enrichment of iPLA2-mediated fatty acid metabolism pathways (e.g., arachidonic acid metabolism). To assess the contribution of iPLA2, animals were administered intracoelomic injections of the iPLA2-specific inhibitor FKGK18 (10 nmol/L), starting 6 hpe and repeated daily. Compared to

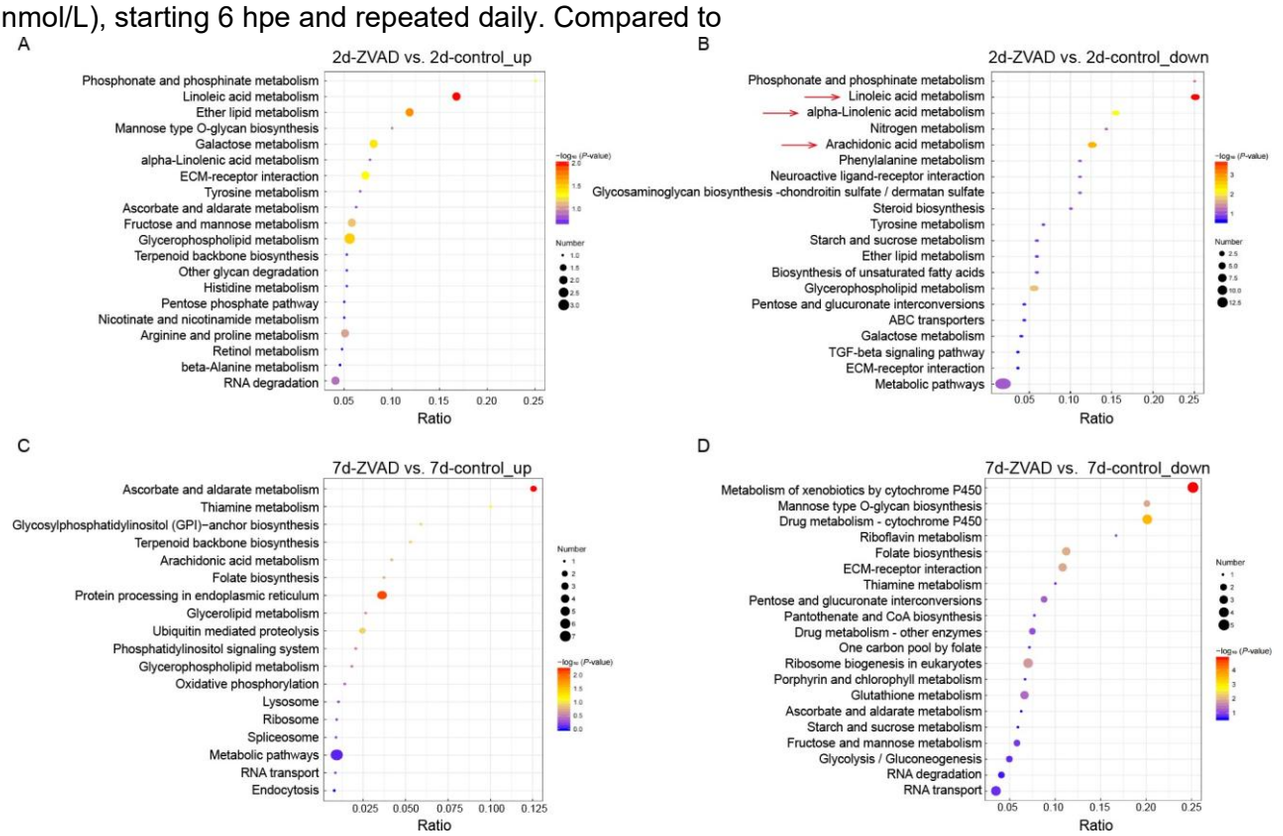

Figure 4 KEGG enrichment analysis of differentially expressed proteins in control and Z-VAD-treated groups

A: Enrichment analysis of up-regulated proteins in 2d_Z-VAD compared to 2d_control. B: Enrichment analysis of down-regulated proteins in 2d_Z- VAD compared to 2d_control. C: Enrichment analysis of up-regulated proteins in 7d_Z-VAD compared to 7d_control. D: Enrichment analysis of down-regulated proteins in 7d_Z-VAD compared to 7d_control.

DMSO-injected controls, FKGK18 significantly impaired regenerative growth, as shown by reduced EdU incorporation and a marked decrease in regenerative primordia size at 7 dpe (Figure 7A). Morphometric quantification of DAPI-stained sections revealed an 82.94% reduction in regenerative primordia area following FKGK18 treatment (P<0.0001) (Figure 7B). Cluster analysis and subsequent validation at both protein and mRNA levels implicated *EGFL7* and *WNT6* signaling in apoptosis-regulated intestinal regeneration. To assess their functional relevance, gene-specific siRNAs targeting *EGFL7* (si*EGFL7)* and *WNT6* (si*WNT6*) were intracoelomically administered beginning at 6 hpe and repeated every 48 h, with negative control siRNA used in parallel. Effective gene silencing was confirmed by qPCR and western blotting (Supplementary Figure S3A–D). At 7 dpe, si*EGFL7* interference led to a 74.89% reduction (P<0.0001) in regenerative primordia area (Figure 7C, D), while si*WNT6* similarly reduced the area by 72.31% (P<0.0001) and significantly decreased EdU^+ cell fluorescence compared with controls (Figure 7E, F). These results indicate that both *EGFL7* and *WNT6* are required for successful intestinal regeneration in *A. japonicus.*

DISCUSSION

Apoptotic dynamics during intestinal regeneration in *A. japonicus* were systematically characterized using TUNEL assays, revealing a tightly coordinated temporal and spatial activation pattern. Under physiological conditions, the basal apoptosis rate was remarkably low, likely reflecting steady- state cellular turnover (Figure 1A). Following evisceration, however, apoptosis levels exhibited dynamic elevation duringcritical regenerative phases, with a pronounced peak at the lumen initiation stage. Significant increases were detected during both mesenteric wound healing and distal mesenteric swelling, suggesting that apoptosis participates throughout the continuum from initial mesenteric repair to primordial lumen formation. This temporal trajectory aligns with apoptotic peaks reported at 7 dpe in *H. glaberrima* (Mashanov et al., 2010; Quispe-Parra et al., 2021). Notably, this study provides the first detailed temporal map of apoptotic dynamics during intestinal regeneration in the sea cucumber, identifying 12 dpe as the critical stage of peak apoptotic activity in *A. japonicus*.

Apoptotic cells were initially localized in the outer mesodermal compartment during early wound closure and structural reorganization but progressively shifted to the inner epithelial layer as rudiment morphogenesis advanced (Figure 1A). This spatial and temporal specificity suggests that apoptosis executes stage-specific functions through different cellular mechanisms—potentially mediating architectural remodeling in mesothelial tissues during early regeneration and driving epithelial reorganization during lumenogenesis. These findings support the emerging paradigm that apoptosis regulates regenerative processes. Comparative insights from other metazoans underscore the conserved yet context-dependent role of apoptosis in regeneration. In planarians, biphasic apoptotic waves coordinate proliferation dynamics post-amputation (Guerin et al., 2021; Pellettieri et al., 2010), while head regeneration in *Hydra* species requires a rapid, spatially restricted apoptotic burst within a critical 30 min window (Chera et al., 2011). In vertebrates, apoptosis contributes to regeneration through stage-specific remodeling. In *Xenopus*, tail regeneration involves apoptosis-driven tissue

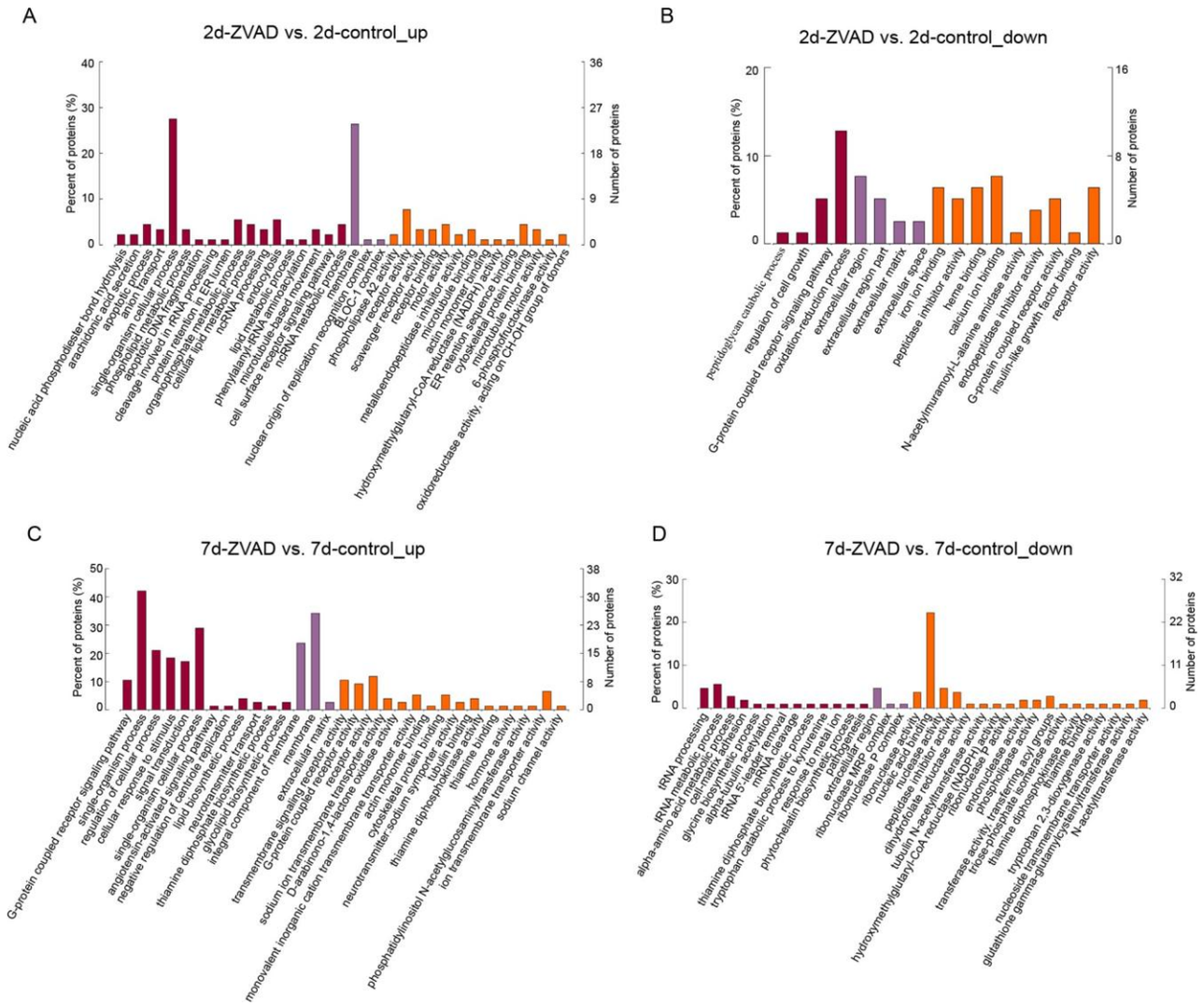

Figure 5 Gene Ontology (GO) analysis of DEPs in control and Z-VAD-treated groups

A: GO analysis of up-regulated proteins in 2d_Z-VAD compared to 2d_control. B: GO analysis of down-regulated proteins in 2d_Z-VAD compared to 2d_control. C: GO analysis of up-regulated proteins in 7d_Z-VAD compared to 7d_control. D: GO analysis of down-regulated proteins in 7d_Z- VAD compared to 7d_control. Red denotes biological process (BP), purple denotes molecular function (MF), and orange denotes cellular component (CC).

reorganization (Tseng et al., 2007), while in zebrafish, fin regeneration displays two apoptotic peaks, with only the later event at 15 h post-injury actively promoting regenerative outgrowth (Gauron et al., 2013; Sehring & Weidinger, 2020). Across evolutionary lineages, the complexity of apoptotic timing and function increases from basal metazoans to vertebrates. Nevertheless, the core involvement of apoptosis in coordinating wound healing and regeneration has remained conserved throughout approximately 550 million years of deuterostome evolution.

Biochemical profiling revealed a temporal discrepancy between caspase activation and apoptotic cell death during intestinal regeneration. Western blot analysis showed elevated levels of cleaved caspase activity at 20 dpe, despite a low frequency of TUNEL-positive cells at this stage (Figure 1E). This divergence aligns with observations in vertebrate systems, where caspase activation can occur independently of cell death, a phenomenon termed non-lethal or non-apoptotic caspase activation (Kuranaga, 2012). Non-lethal caspase activation has been implicated in diverse cellular processes, including proliferation, fate determination, differentiation,migration, secretion, and cytoskeletal remodeling, in a tissue- specific manner (Baena-Lopez et al., 2018; Kuranaga, 2012; Li & Yuan, 2008;

Miura, 2012; Mukherjee & Williams, 2017; Nakajima & Kuranaga, 2017; Yi & Yuan, 2009). Notably, spatial regulation of caspase activation has been shown to confer functional specificity, as illustrated by caspase-3 activation in the absence of apoptosis within leading-edge cells during thorax closure in *Drosophila* pupae (Fujisawa et al., 2019). Similarly, in *Drosophila* wing discs, a subset of necrosis-induced apoptosis (NiA) cells remain viable post- caspase activation and contributes to compensatory proliferation during late-stage necrosis-induced regeneration (Klemm et al., 2024). Although our findings suggest a comparable phenomenon may occur late in intestinal regeneration in *A. japonicus*, this has not been previously reported in invertebrates, and its function requires further investigation.

To further elucidate the functional relevance of apoptosis during early regeneration, the pan-caspase inhibitor Z-VAD was administered intracoelomically. Inhibition of caspase activity resulted in a delay

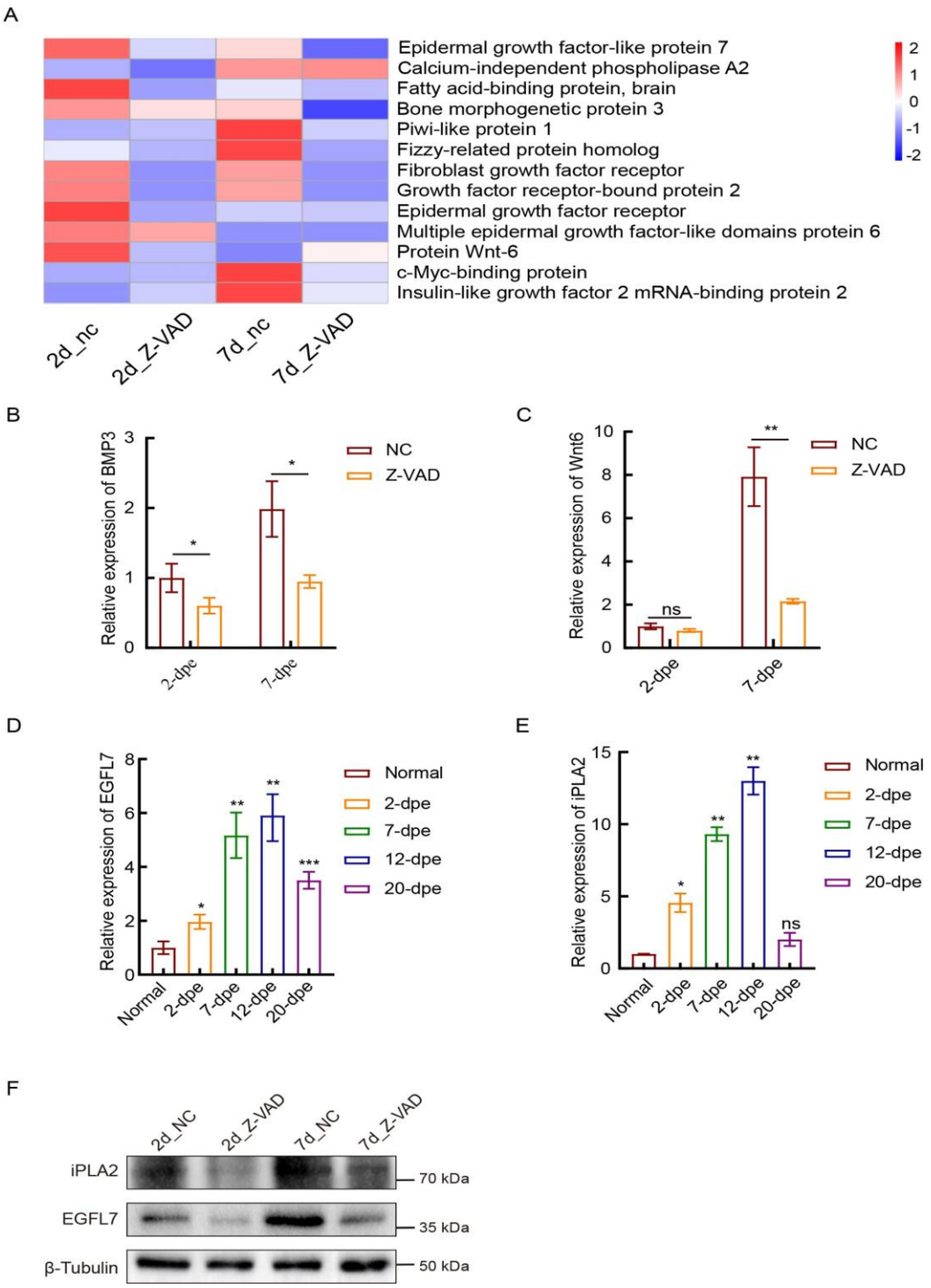

Figure 6 Expression pattern analysis of regeneration-related proteins following apoptosis inhibition

A: Heatmap showing correlation analysis of regeneration-related proteins. 2d_nc and 2d_Z-VAD denote 2d_control and 2d Z-VAD groups, respectively; 7d_nc and 7d_Z-VAD denote 7d_control and 7d Z-VAD groups, respectively. B: qPCR analysis of BMP3 mRNA expression in control and apoptosis-inhibited groups. C: qPCR analysis of WNT6 mRNA expression in control and apoptosis-inhibited groups. D: qPCR analysis of EGFL7 mRNA expression across different regeneration time points. E: qPCR analysis of iPLA2 mRNA expression across different regeneration time points. F: Protein expression of iPLA2 and EGFL7 in control and Z-VAD-treated groups at 2 dpe and 7 dpe, with β-tubulin as the internal reference. dpe: days post-evisceration. Data represent mean±SD, n=3 independent individuals; ns: Not significant; *: P<0.05; **: P<0.01.

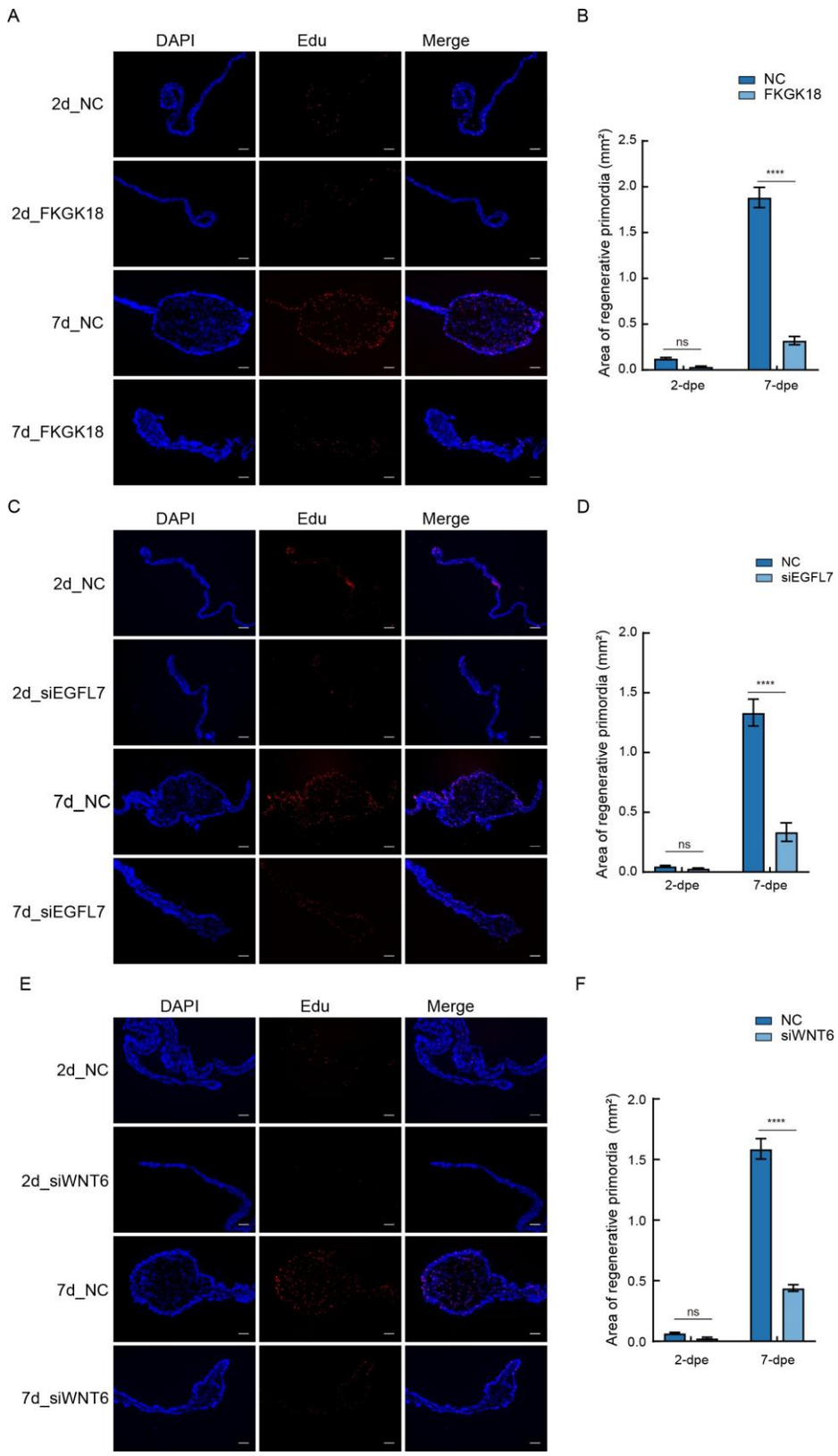

Figure 7 Inhibition of iPLA2, EGFL7, and WNT6 significantly impairs intestinal regenerative primordial remodeling

A: Detection of intestinal regeneration and cell proliferation after EGFL7 interference using EdU *in situ* hybridization; blue, DAPI-stained nuclei; red, EdU-stained proliferating cells. Scale bar: 200 μm. B: Quantification of regenerative primordia area from DAPI-stained sections in A. C: Assessment of proliferative activity and intestinal regeneration following iPLA2 inhibition using EdU *in situ* hybridization; DAPI (blue), EdU (red). Scale bar: 200 μm. D: Quantification of regenerative primordia area from DAPI-stained sections in C. E: Detection of intestinal regeneration and cell

proliferation after WNT6 interference by EdU *in situ* hybridization; DAPI (blue), EdU (red). Scale bar: 200 μm. F: Statistical analysis of intestinal regenerative primordia area from DAPI in E. Statistical analyses represent mean±SD (*n*=3 independent experiments); ns: Not significant; ****: *P*<0.0001.

progression. Previous studies in *H. glaberrima* have reported that the administration of Z-VAD (20 μmol/L and 40 μmol/L) reduces cell proliferation during early intestinal regeneration but does not significantly affect regenerative progenitor growth, leading to the hypothesis that complete apoptotic blockade arrests regeneration (Reyes-Rivera et al., 2024). Consistent with this hypothesis, Z-VAD treatment at a higher concentration (100 μmol/L) in *A. japonicus* significantly inhibited regenerative rudiment growth, arrested apoptosis at basal levels, and suppressed the expression of key regeneration-related genes, including *WNT6*, *EGFL7*, and *BMP3*. Similar dependencies have been reported in vertebrates. For example, caspase-3 inhibition blocks tail regeneration in *Xenopus laevis* tadpoles via disruption of Wnt/β-catenin signaling (Tseng et al., 2007), while apoptosis is essential for blastema formation and zebrafish fin regeneration (Gauron et al., 2013). Caspase-3/7 activity is likewise required for effective liver repair in mammals (Li et al., 2010). Collectively, these findings indicate a conserved requirement for apoptosis signaling in regenerative processes across taxa.

Despite growing recognition of apoptosis as a regulatory mechanism in regeneration, the molecular mechanisms through which it exerts these effects are still poorly understood. To investigate this, proteomic profiling of *A. japonicus* intestinal tissue was conducted at two critical regenerative stages following Z-VAD-mediated apoptosis inhibition. The five most significantly down-regulated proteins at 2 dpe or 7 dpe included fatty acid-binding proteins FABP7 and FABP6, suggesting a potential link between apoptosis and lipid metabolism. KEGG pathway analysis revealed significant suppression of lipid-mediated signaling cascades at
2 dpe, particularly those involved in arachidonic acid metabolism, linoleic acid metabolism, and glycerophospholipid metabolism. These pathways are known to generate bioactive lipid mediators such as prostaglandin E2 (PGE2) and leukotriene B4 (LTB4), which promote tissue repair by activating Wnt/β-catenin signaling and stimulating progenitor expansion (Lauber et al., 2003; Leng & Jiang, 2019; Wang et al., 2020). These findings are consistent with observations in mammals, where apoptosis-dependent arachidonic acid flux is essential for hepatic regeneration (Li et al., 2010). Concurrent suppression of glycerophospholipid biosynthesis may impair membrane biogenesis, as phospholipid availability directly governs S-phase entry and cell cycle progression during morphogenesis (Meehan et al., 2023). By 7 dpe, coinciding with distal mesenteric expansion, apoptosis inhibition disrupted pathways involved in redox regulation and energy metabolism, including folate biosynthesis, glutathione metabolism, and glycolysis/gluconeogenesis. Folate serves as an essential coenzyme for nucleotide biosynthesis, amino acid metabolism, and methylation reactions (Barbiroli et al., 1975) and promotes regenerative processes in mammalian liver and central nervous system tissues via epigenetic reprogramming (Barbiroli et al., 1975; Zhang et al., 2008). Glutathione binds amino acid transporters, facilitates amino acid uptake, supports amino acid metabolism, and provides cellular building blocks (Aoyama, 2021). It also protects mitochondria from oxidative damage, maintains mitochondrial function, and supports cell division, migration, and ECM synthesis (Wang et al., 2024). These findings suggest that apoptosis may modulate intestinal regeneration not only by enabling structural remodeling but also by orchestrating the metabolicenvironment required for cellular growth, with a particularly prominent role in fatty acid-mediated signaling and biosynthetic support.

To clarify the molecular mechanisms underlying apoptosis- regulated regeneration, heatmap profiling of regeneration- associated proteins was conducted across key post-evisceration phases in *A. japonicus*. Suppression of apoptosis resulted in marked down-regulation of PIWIL1, a conserved stem

cell marker implicated in the maintenance of progenitor cell populations in various metazoans, including planarian neoblasts and cnidarian mesenchymal cells (van Wolfswinkel, 2014). This observation extends recent reports on the presence of $PIWIL1^+$ coelomocyte populations in *A. japonicus* (Zavalnaya et al., 2020), reinforcing the hypothesis that stem/progenitor cell lineages are engaged in *A. japonicus* intestinal regeneration. In addition, apoptotic blockade also significantly suppressed Ca^{2+}-iPLA2 expression. KEGG pathway enrichment analysis revealed significant down- regulation of iPLA2-regulated lipid signaling cascades, particularly those involved in arachidonic acid metabolism (Figure 4), consistent with the observed suppression of FABP7 and FABP6 expression following Z-VAD treatment. Previous studies have demonstrated that iPLA2 is activated downstream of caspase-3 during apoptosis, mediating fatty acid mobilization essential for cell migration and proliferation (Ma & Turk, 2001; Li et al., 2010). The functional significance of iPLA2 in regeneration was validated experimentally: its inhibition impaired intestinal regrowth, while apoptosis suppression reduced both protein and mRNA levels of iPLA2 (Figure 7A, B; Supplementary Figure S4D), implicating iPLA2 as a critical downstream effector of apoptosis-regulated lipid signaling (Figure 8). Despite these insights, comprehensive profiling of terminal lipid mediators, such as eicosanoids, lysophospholipids, and PGE2, remains essential to delineate specific signaling events. In vertebrate systems, apoptosis- mediated lipid signaling regulates cell migration and proliferation. For example, apoptotic cells secrete lysophosphatidylcholine, which recruits THP-1 cells to apoptotic MCF7 cells via a caspase-3-dependent mechanism (Lauber et al., 2003). Similarly, *caspase-3*-mediated *iPLA2* activation generates arachidonic acid release, enhancing the migration of non-apoptotic ovarian cancer cells in humans (Zhao et al., 2006). In the regenerating mouse liver, *caspase- 3/7* knockdown impairs tissue regrowth, whereas arachidonic acid derived through the same enzymatic axis restores regenerative capacity by promoting progenitor and stem cell expansion (Li et al., 2010). Furthermore, apoptotic metabolites have been shown to reprogram transcriptomes of neighboring viable cells, modulating inflammation, proliferation, and vesicular trafficking (Medina et al., 2020). Collectively, these findings indicate that a similar apoptosis-iPLA2-lipid signaling axis may regulate regeneration in invertebrates, although its biological function and molecular mechanisms require further investigation.

In invertebrate regeneration models, such as *Hydra* and *Ciona*, WNT3 functions as a canonical effector of apoptosis- triggered regeneration (Chera et al., 2009; Jeffery & Gorički, 2021). In contrast, heatmap analysis during intestinal regeneration in *A. japonicus* revealed that WNT6, not WNT3, was the principal WNT ligand significantly down-regulated following apoptosis inhibition. We found that apoptosis inhibition substantially suppressed WNT6 expression (Figure 6A, C). This repression was further validated by

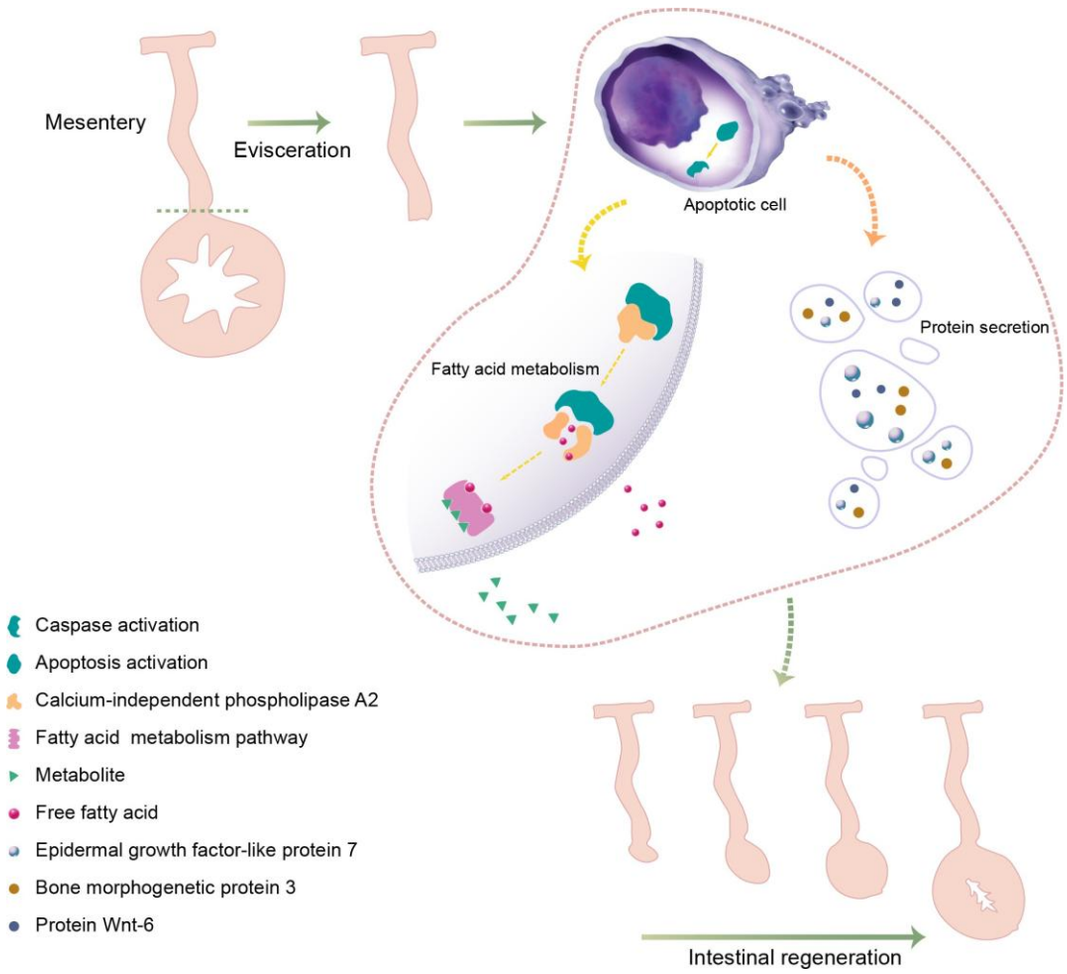

Figure 8 Schematic of two hypothetical pathways of apoptosis-regulated regeneration

In spontaneous evisceration of *A. japonicus*, apoptosis activation in damaged tissue occurs with caspase activation and apoptotic vesicle secretion. Caspases may activate iPLA2-dependent fatty acid metabolism, generating free fatty acids that support regeneration. Apoptotic cells may also secrete regeneration-associated proteins such as EGFL7 and WNT6 in extracellular vesicles to promote intestinal regeneration.

functional knockdown. Notably, RNA interference targeting WNT6 led to marked reductions in regenerative primordia area and proliferative cell counts during critical morphogenetic stages (Figure 7C). These findings align with prior observations that WNT6 expression is up-regulated during intestinal regeneration in both *A. japonicus and H. glaberrima* (Auger et al., 2023), highlighting the conserved regulatory function of Wnt/β-catenin signaling in echinoderm regeneration. Wnt/β-catenin signaling is broadly required for proliferative control in echinoderm regeneration, demonstrated by its function in *H. glaberrima* intestinal repair (Alicea- Delgado & García-Arrarás, 2021; Auger et al., 2023). In *Hydra*, apoptotic cells at the wound site release WNT3 to stimulate proliferation in neighboring cells, driving head regeneration (Galliot & Chera, 2010). In *Ciona*, caspase inhibition disrupts progenitor cell survival and oral siphon regeneration, while WNT3a rescues the effects of caspase inhibition on oral siphon regeneration and branchial sac homeostasis (Jeffery & Gorički, 2021). The reliance on WNT6 rather than WNT3 in *A. japonicus* suggests an evolutionary shift in apoptotic Wnt effectors, reflecting lineage-specific adaptations of a conserved regenerative mechanism. In vertebrate systems, apoptosis similarly acts as a signal for compensatory proliferation. For example, reactive oxygen species (ROS)-induced apoptosis is required for regenerative outgrowth in zebrafish fins by promoting proliferation of stump epidermal cells (Gauron et al., 2013). In murine liver, dying hepatocytes secrete interleukin-11 (IL-11), triggering JAK/STAT signaling in healthy hepatocytes to initiate repair following acute injury (Nishina et al., 2012). These diverse models illustrate that while the apoptotic trigger for regeneration is conserved across metazoans, the molecular mediators—ranging from specific Wnt ligands to cytokine signals—are subject to evolutionary divergence and tissue- specific regulation.

Emerging evidence indicates that apoptosis modulates the regenerative microenvironment via paracrine release of specific metabolites and growth factors (Brandel et al., 2022; Medina et al., 2020; Ye et al., 2023). In *A. japonicus*, inhibition of apoptosis resulted in stage-specific repression of several key regenerative growth factors and their signaling components, including BMP3, EGFL7, and growth factor receptor-binding protein. Among these, EGFL7 was significantly down-regulated at both 2 dpe and 7 dpe following apoptosis inhibition (Figure 6A, F), suggesting its critical regulatory function. RNA interference targeting EGFL7 significantly impaired regenerative progression (Figure 7A, B), underscoring its functional relevance. This finding aligns with vertebrate models, in which EGFL7 supports tissue regeneration by promoting osteoblast differentiation and influencing epidermal stem cell migration and proliferation via Notch signaling (Chang et al., 2023; Zhang et al., 2023). A lausible mechanistic link between apoptosis and regeneration may include apoptotic vesicle-mediated signaling. Apoptotic cells release extracellular vesicles containing proteins and nucleic acids that shape the surrounding microenvironment, contributing to tissue repair, immune regulation, and disease processes. In mammalian liver regeneration, apoptotic signaling triggers the secretion of HGF, basic fibroblast growth factor (bFGF), and VEGF, all of which promote tissue repair (Brandel et al., 2022). By analogy, our results suggest that apoptotic cells in *A. japonicus* may regulate regeneration by releasing pro-regenerative factors such as EGFL7 and WNT6 (Figure 8). The temporal suppression of these factors following apoptosis inhibition supports this hypothesis. Despite extensive data from vertebrate systems, apoptotic vesicle signaling in invertebrate regeneration remains poorly characterized. Future work should prioritize: (1) isolation and characterization of apoptotic vesicles during echinoderm regeneration, (2) experimental elucidation of functional relationships between vesicle-derived cargo, particularly EGFL7 and WNT6, and recipient cell responses, and (3) comparative analyses across taxa to define conserved and divergent modes of vesicle-mediated signaling. These studies will improve our understanding of regeneration mechanisms at the cellular and molecular levels

and may reveal general principles governing tissue repair across metazoans.

Apoptosis has been reported to regulate several biological processes, including cell dedifferentiation, proliferation, and migration (Bergmann & Steller, 2010; Codispoti et al., 2019). Proteomic sequencing and preliminary functional assays in *A. japonicus* demonstrated that apoptosis participated in intestinal regeneration through Ca^{2+}-iPLA2 and EGFL7/WNT6 signaling. Previous studies have shown that iPLA2-mediated lipid signaling promotes cell migration and proliferation by facilitating the production of lysophosphatidylcholine and PGE2 (Hooks & Cummings, 2008; Lauber et al., 2003; Li et al., 2010). EGFL7, originally identified for its role in tubulogenesis and angiogenesis, modulates cellular migration and proliferation during tissue remodeling (Chang et al., 2023; de Oliveira et al., 2023). WNT signaling, a well-established pathway for regulating cell proliferation, has also been described in multiple regeneration models (Alicea-Delgado & García-Arrarás, 2021; Auger et al., 2023; Hayat et al., 2022; Li et al., 2017). Collectively, these data suggest that apoptosis may control regeneration in *A. japonicus* by orchestrating proliferative and migratory responses through metabolic and signaling networks. Targeted investigations into these pathways and their downstream effects on cellular reprogramming and lineage specification represent an important direction for future research.

This study demonstrates the essential role of apoptotic activity in *A. japonicus* intestinal regeneration. Integrated proteomic profiling and gene perturbation experiments support two mechanistic models: caspase-mediated metabolic reprogramming through lipid mediators and apoptosis- dependent growth signaling via WNT6 and EGFL7. These mechanisms provide novel insight into the molecular basis of echinoderm regeneration and expand current understanding of apoptotic function beyond cell elimination. However, the regulatory frameworks proposed herein remain to be functionally validated *in vivo*. The findings lay a foundation for comparative analyses across metazoans to determine the evolutionary conservation of these regenerative programs.Moreover, elucidating the mechanisms by which apoptosis coordinates tissue remodeling in marine invertebrates may offer translational potential for therapeutic strategies targeting hepatic, intestinal, and dermal regeneration in mammals.

SUPPLEMENTARY DATA

Supplementary data to this article can be found online.

COMPETING INTERESTS

The authors declare that they have no competing interests.

AUTHORS' CONTRIBUTIONS

K.X conducted the experiments, processed the data, and drafted the manuscript. X.Z. conducted part of the experiments. C.L.Z participated in the experimental design and revised the manuscript. C.H.L. designed the study and provided reagents and analytical tools. All authors read and approved the final version of the manuscript.

REFERENCES

Alicea-Delgado M, García-Arrarás JE. 2021. Wnt/β-catenin signaling pathway regulates cell proliferation but not muscle dedifferentiation nor apoptosis during sea cucumber intestinal regeneration. *Developmental Biology*, **480**: 105–113.

Aoyama K. 2021. Glutathione in the brain. *International Journal of Molecular Sciences*, **22**(9): 5010.

Auger NA, Medina-Feliciano JG, Quispe-Parra DJ, et al. 2023. Characterization and expression of holothurian Wnt signaling genes during adult intestinal organogenesis. *Genes*, **14**(2): 309.

Baena-Lopez LA, Arthurton L, Xu DC, et al. 2018.

Non-apoptotic caspase regulation of stem cell properties. *Seminars in Cell & Developmental Biology*, **82**: 118–126.

Barbiroli B, Bovina C, Tolomelli B, et al. 1975. Folate metabolism in the rat liver during regeneration after partial hepatectomy. *Biochemical Journal*, **152**(2): 229–232.

Bergmann A, Steller H. 2010. Apoptosis, stem cells, and tissue regeneration. *Science Signaling*, **3**(145): re8.

Boada-Romero E, Martinez J, Heckmann BL, et al. 2020. The clearance of dead cells by efferocytosis. *Nature Reviews Molecular Cell Biology*, **21**(7): 398–414.

Böttger A, Alexandrova O. 2007. Programmed cell death in *Hydra*. *Seminars in Cancer Biology*, **17**(2): 134–146.

Brandel V, Schimek V, Göber S, et al. 2022. Hepatectomy-induced apoptotic extracellular vesicles stimulate neutrophils to secrete regenerative growth factors. *Journal of Hepatology*, **77**(6): 1619–1630.

Brockes JP, Kumar A. 2008. Comparative aspects of animal regeneration. *Annual Review of Cell and Developmental Biology*, **24**: 525–549.

Chang JY, Sun Y, Meng XX, et al. 2023. EGFL7 affects the migration of epidermal stem cells in refractory diabetic wounds by regulating notch signaling pathway. *Regenerative Medicine*, **18**(2): 137–153.

Chera S, Ghila L, Dobretz K, et al. 2009. Apoptotic cells provide an unexpected source of Wnt3 signaling to drive *Hydra* head regeneration. *Developmental Cell*, **17**(2): 279–289.

Chera S, Ghila L, Wenger Y, et al. 2011. Injury-induced activation of the MAPK/CREB pathway triggers apoptosis-induced compensatory proliferation in hydra head regeneration. *Development, Growth & Differentiation*, **53**(2): 186–201.

Codispoti B, Makeeva I, Sied J, et al. 2019. Should we reconsider the apoptosis as a strategic player in tissue regeneration?. *International Journal of Biological Sciences*, **15**(10): 2029–2036.

de Oliveira C, Gonçalves PG, Bidinotto LT. 2023. Role of EGFL7 in human cancers: a review. *Journal of Cellular Physiology*, **238**(8): 1756–1767.

Eisapour M, Salamat N, Salari MA, et al. 2021. Digestive tract regeneration in the sea cucumber Holothuria parva, which is posteriorly eviscerating (Holothuroidea, Echinodermata). 69–83 in Zoomorphology, 140(1).

Elmore, S. (2007). A review on planned cell death: apoptosis. 35(4), Toxicologic Pathology, 495–516.

Kosakamoto H, Chihara T, Fujisawa Y, et al. 2019. Drosophila caspase activation's non-apoptotic role in wound healing and epithelial thorax closure. Development, 146(4): dev169037.

Chera S., Galliot B. (2010). The Hydra model: revealing a Wnt-based regeneration generator powered by apoptosis. Cell Biology Trends, 20(9): 514–523.

Bello SA, Malavez S, García-Arrarás JE. 2019. The hub of intestinal regeneration is the mesentery. Cell & Developmental Biology Seminars, 92: 45–54.

Gauron C, Bouzaffour M, Rampon C, et al. (2013). Continuous ROS creation is necessary for regeneration to occur because it sets off compensatory proliferation. 2084 in Scientific Reports, 3(1).

Tseng KAS, Kha CX, and Guerin DJ. 2021. After injury, cell death gives way to regeneration. Cell and Developmental Biology Frontiers, 9: 655048.

Li X, Tao WJ, Guo M, et al. 2024. In Apostichopus japonicus, Vibrio splendidus infection stimulates circRNA-FGL1-regulated coelomocyte death via competitively binding to Myc with the deubiquitinase OTUB1. e1012463 in PLoS Pathogens, 20(8).

Fu XM, Guo M, Wang YK, et al. 2023. In response to Vibrio splendidus infection, circRNA1149 from Apostichopus japonicus inhibits coelomocyte death and functions as a miR-92a sponge to control Bax expression. 738812 in Aquaculture, 562.

Manzoor M, Hussain A, and Hayat R. 2022. A

thorough analysis of the Wnt signaling pathway. International Cell Biology, 46(6): 863–877. Cummings BS, Hooks SB. 2008. Ca2+-independent phospholipase A2's function in signaling and cell proliferation. 1059–1067 in Biochemical Pharmacology, 76(9). Lempicki RA, Huang DW, and Sherman BT. 2009. Tools for bioinformatics enrichment: avenues for thorough functional study of extensive gene lists. Research on Nucleic Acids, 37(1): 1–13. Gorički Š, Jeffrey WR. 2021. In the ascidian Ciona, apoptosis is a catalyst for both homeostatic cell renewal and Wnt-dependent regeneration. Bio058526 in Biology Open, 10(4). Chang HY, Jones P, Binns D, et al. 2014. InterProScan 5: categorization of protein functions at the genome scale. 30(9), Bioinformatics, 1236–1240. Harris RE, Klemm JW, and van Hazel C. 2024. Non-apoptotic caspase activity mediates regeneration after tissue necrosis. https://doi.org/10.1101/2024.07.26.605350, BioRxiv.
Kuranaga E. (2012). Caspases' in vivo regulation mechanisms and functions extend beyond apoptosis. 83–97 in Genes to Cells, 17(2). Lauber K, Kröber SM, Bohn E, et al. (2003). Through the release of a lipid attraction signal mediated by caspase-3, apoptotic cells cause phagocyte migration. 717–730 in Cell, 113(6). Jiang H. and Leng X. 2019. effects of arachidonic acid and its main prostaglandin derivatives on the fusion, differentiation, and proliferation of bovine myoblasts. Endocrinology of Domestic Animals, 67: 28–36.
Huang Q, Chen J, Li F, et al. (2010). The "phoenix rising" pathway is triggered by apoptotic cells to encourage tissue regeneration and wound repair. Signaling Science, 3(110): ra13. Li J, Yuan J. (2008). apoptotic and other caspases. 27(48): 6194–6206; Oncogene. Yang HS, Li XN, Sun LN, et al. 2017. The sea cucumber Apostichopus japonicus exhibits intestinal regeneration, and WntA expression is identified and characterized. Biochemistry and Molecular Biology, Part B of Comparative Biochemistry and Physiology, 210: 55–63. Schmittgen TD, Livak KJ. 2001. Relative gene expression data analysis

utilizing the 2-ΔΔCT technique and real-time quantitative PCR. 25(4), Methods: 402–408. Turk J., Ma ZM. 2001. The group VIA's molecular biology Phospholipase A2 is independent of Ca2+. Molecular Biology and Nucleic Acid Research Progress, 67: 1–33. Maden M. (2018). What does the evolution of regeneration mean for mammals? 62(6–8): 369–372 in The International Journal of Developmental Biology.
Rojas-Catagena C, Zueva OR, Mashanov VS, et al. (2010). The mesothelium of sea cucumbers expresses survivin and mortalin homologs extensively during visceral regeneration. 10(1): 117 in BMC Developmental Biology. Arandjelovic S, Mehrotra P, Medina CB, et al. 2020. Apoptotic cells emit metabolites that function as tissue messengers. 130–135 in Nature, 580(7801). García-Arrarás JE, Medina-Feliciano JG. 2021. Molecular developments in echinoderm regeneration. Cell and Developmental Biology Frontiers, 9: 768641. Meehan SD, Bhattacharya SK, Neag E. 2023. Potential membrane order modifications linked to the lipidomic shifts are shown by glycerophospholipid analysis of optic nerve regeneration models. 39(8): 519–529 in Journal of Ocular Pharmacology and Therapeutics. Miura M. (2012). Animal development involves both apoptotic and nonapoptotic caspase activities. Perspectives in Biology, Cold Spring Harbor, 4(10): a008664. Williams DW, Mukherjee A. 2017. More alive than dead: caspases' non-apoptotic functions in illness, brain development, and plasticity. Differentiation & Cell Death, 24(8): 1411–1421.
Kuranaga E. and Nakajima YI. 2017. non-apoptotic pathways in development that rely on caspase. Differentiation & Cell Death, 24(8): 1422–1430. Yanaka S, Nishina T, Komazawa-Sakon S, et al. (2012). Oxidative stress and compensatory proliferation are linked by interleukin-11. ra5 in Science Signaling, 5(207). Pellettieri J, Watanabe S, Fitzgerald P, et al. (2010). In planarian regeneration, tissue remodeling and cell death occur. 76–85 in Developmental Biology, 338(1).

García-Arrarás JE, Quispe-Parra D, and Valentín G. 2021. An intestinal regeneration route map. 65(4-6): 427–437 in The International Journal of Developmental Biology.
Grillo-Alvarado V, Soriano-López AE, Reyes-Rivera J, et al. 2024. There is proof that apoptosis, cell division, and dedifferentiation interact in the rudiment during the sea cucumber's whole-organ intestinal regeneration. 99–109 in Developmental Biology, 505.
García-Arrarás JE, San Miguel-Ruiz JE. 2007. In the sea cucumber Holothuria glaberrima, common cellular processes take place during wound healing and organ regeneration. Developmental Biology, BMC, 7(1): 115.
Alvarado A. Sánchez. 2006. Planarian regeneration: the beginning is the end. 124(2): 241–245 in Cell.
Weidinger G., Sehring IM. 2020. recent developments in our knowledge of zebrafish fin regeneration. 9(1): e367 in WIREs Developmental Biology.
Qiu DY, Tseng AS, Adams DS, et al. 2007. In the early phases of Xenopus laevis tail regeneration, apoptosis is necessary. 62–69 in Developmental Biology, 301(1).
Zhang Z, Tu WT, Guo M, et al. 2024. A review of pathogen-induced apoptosis in echinoderms. Immunology of Fish and Shellfish, 155: 109990.
JC van Wolfswinkel. 2014. Piwi and potency: PIWI proteins in regeneration and animal stem cells. 54(4): 700–713 in Integrative and Comparative Biology.
Galliot B, Reiter S, and Vriz S. 2014. Cell death: a regeneration program. Developmental Biology: Current Topics, 108: 121–151.
Jiang JW, Wang DH, Wang MY, and others (2024). Mitophagy stimulates glutathione metabolism, which aids in hair regrowth. Research, 7: 0433.
Sheng XL, Wang QY, Lin YY, et al. 2020. Arachidonic acid encourages